Earth and Planetary Science Letters 300 (2010) 395–401

Contents lists available at ScienceDirect

Earth and Planetary Science Letters

journal homepage: www.elsevier.com/locate/epsl

Crustal structure of the Gamburtsev Mountains, East Antarctica, from S-wave receiver functions and Rayleigh wave phase velocities

Samantha E. Hansen [a,*], Andrew A. Nyblade [b], David S. Heeszel [c], Douglas A. Wiens [c], Patrick Shore [c], Masaki Kanao [d]

[a] Dept. of Geological Sciences, University of Alabama, Tuscaloosa, AL 35487, USA
[b] Dept. of Geosciences, Pennsylvania State University, University Park, PA 16802, USA
[c] Dept. of Earth and Planetary Sciences, Washington University in St. Louis, St. Louis, MO 63130, USA
[d] Geoscience Research Group and Polar Data Center, National Institute of Polar Research, Tokyo, 190-8518, Japan

ARTICLE INFO

Article history:
Received 21 July 2010
Received in revised form 5 October 2010
Accepted 17 October 2010
Available online 13 November 2010

Editor: R.D. van der Hilst

Keywords:
Gamburtsev Mountains
Antarctica
crustal structure
S-wave receiver functions

ABSTRACT

The Gamburtsev Subglacial Mountains (GSM), located in central East Antarctica, are one of the most enigmatic tectonic features on Earth. Buried beneath several kilometers of ice, the mountains are characterized by peak elevations reaching ~3000 m above sea level. In this study, new data from the Gamburtsev Antarctic Mountains Seismic Experiment (GAMSEIS) are presented, which substantially improve constraints on the crustal and upper mantle structure in this region. S-wave receiver functions and Rayleigh wave phase velocities are used to analyze data from the GAMSEIS deployment and to improve estimates of crustal thickness beneath the East Antarctic craton and the GSM. Our results indicate that the cratonic crust surrounding the GSM is ~40–45 km thick. Beneath the GSM, the crust thickens to ~55–58 km and provides isostatic support for the high mountain elevations. It has been suggested that thicker crust beneath the GSM may reflect magmatic underplating associated with a mantle plume. However, considering our results with those from other previous and ongoing studies, we instead favor models in which the GSM are an old continental feature associated with either Proterozoic or Paleozoic tectonic events.

1. Introduction

Located near the center of East Antarctica are the Gamburtsev Subglacial Mountains (GSM), which are characterized by some of the highest bedrock elevations (~2500 m) on the continent (Cogley, 1984; DeConto and Pollard, 2003). The GSM are of great interest since they may have served as a nucleation point for the first large-scale ice sheets that formed in Antarctica as the Earth's climate cooled ~34 Ma (Bo et al., 2009; DeConto and Pollard, 2003). Yet, with only limited constraints available on the topography, geology, and lithospheric structure, the origin of the GSM within the framework of Antarctic tectonics has been a matter of considerable speculation. With no rock samples available, geochronologic constraints on the age of the GSM have not been acquired. Some studies have suggested that the GSM were uplifted by a mantle plume, forming a volcano-capped dome, similar to the Hoggar massif in Africa (Sleep, 2006). Other studies have suggested that the GSM developed through multiple Proterozoic or early Paleozoic orogenic events associated with the assembly of Gondwana (Fitzsimons, 2000, 2003; Liu et al., 2002, 2006; Zhao et al., 1995). Alternatively, the GSM may have resulted from far-field compression associated with the formation of Pangaea during the late Carboniferous–early Permian (Veevers, 1994; Veevers et al., 2008).

Crustal and upper mantle structure provide important constraints needed to decipher the tectonic history of East Antarctica and the GSM; however, little is known. Across the East Antarctic (EA) craton, gravity and seismic studies find an average crustal thickness of ~35–45 km (Bentley, 1991; Block et al., 2009; Hansen et al., 2009; Lawrence et al., 2006; Llubes et al., 2003; Reading, 2006). Surface and body wave velocity studies have indicated a seismically fast upper mantle beneath East Antarctica, consistent with cratonic regions elsewhere in the world (e.g. Morelli and Danesi, 2004; Ritzwoller et al., 2001; Roult and Rouland, 1992), but the spatial resolution of these studies is ~600–1000 km, providing only broad images of the upper mantle structure. Beneath the GSM, the only previous estimates of crustal thickness are from gravimetric or satellite data (Block et al., 2009; Groushinsky and Sazhina, 1982a; von Frese et al., 1999) and vary over a wide range (~42 to 65 km).

With the deployment of the Gamburtsev Antarctic Mountains Seismic Experiment (GAMSEIS), new data are available to investigate the crustal and upper mantle structure in this region further. Often, P-wave receiver functions (PRFs) are used to obtain high frequency

* Corresponding author. University of Alabama, Dept. of Geological Sciences, Box 870338, Tuscaloosa, AL 35487, USA. Tel.: +1 205 348 7089; fax: +1 205 348 0818.
E-mail addresses: shansen@geo.ua.edu (S.E. Hansen), aan2@psu.edu (A.A. Nyblade), davidh@mantle.wustl.edu (D.S. Heeszel), doug@wustl.edu (D.A. Wiens), patrick@mantle.wustl.edu (P. Shore), kanao@nipr.ac.jp (M. Kanao).

0012-821X/$ – see front matter © 2010 Elsevier B.V. All rights reserved.
doi:10.1016/j.epsl.2010.10.022

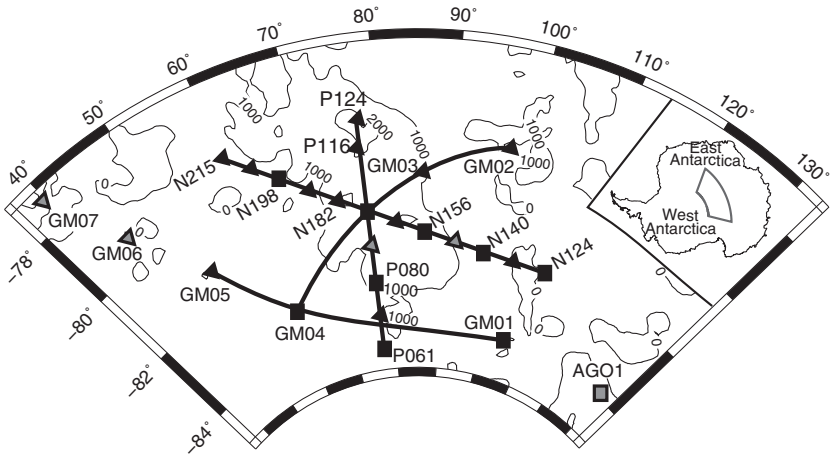

Fig. 1. Map of the GAMSEIS seismic stations. Stations installed during 2007 are shown by squares, and stations installed during 2008–2009 are shown by triangles. Shapes with gray centers denote stations that did not record enough useable data to generate a stack with a high signal-to-noise ratio. Thin lines denote bedrock topography contours from BEDMAP (Lythe et al., 2001) every 1000 m. Several profiles are highlighted by bold lines: the north–south (NS) profile extending from station N124 to station N215, the pole (P) profile extending from station P061 to station P124, the Gamburtsev South (GS) profile extending from station GM01 to stations GM05, and the east–west (EW) profile extending from station GM02 to station GM04.

point measurements of crustal thickness (e.g. Langston, 1979; Zhu and Kanamori, 2000). However, for seismic stations deployed on ice sheets, such as the GAMSEIS stations, determining crustal structure using PRFs can be difficult since ice reverberations may mask P-to-S conversions from the crust–mantle boundary (Moho). On the other hand, S-to-P conversions from the Moho on S-wave receiver functions (SRFs) can be more easily identified because they arrive earlier than the direct S phase while all ice multiples arrive later, making SRFs well suited for investigating crustal structure beneath ice sheets (Hansen et al., 2009). In this study, we use the SRF technique to analyze new data from the GAMSEIS deployment to improve estimates of crustal thickness beneath the GSM and the EA craton. To further constrain the SRFs, Rayleigh wave phase velocities from surface wave tomography are also incorporated into our analysis (Heeszel et al., 2010). Our crustal thickness estimates are then combined with results from previous and ongoing studies to assess proposed origin models for the GSM.

2. Data and methodology

GAMSEIS is a component of the Antarctic Gamburtsev Province (AGAP) International Polar Year project. Originally, in 2007, 10 broadband seismic stations were deployed across the GSM and the EA craton. In December 2008–January 2009, an additional 16 stations were added (Fig. 1), and the full dataset became available in early 2010. Two of the GAMSEIS stations, N124 and N132, were installed at sites previously occupied by the Transantarctic Mountains Seismic Experiment (TAMSEIS), which operated from December 2001 to December 2003 (Lawrence et al., 2006; Watson et al., 2006). A detailed discussion of the SRF technique is provided by Hansen et al. (2009), who used the approach with TAMSEIS data to examine the crustal structure beneath the Transantarctic Mountain range. This methodology will be summarized in the following sections.

2.1. SRF technique

To generate the SRFs, we selected S-waves with high signal-to-noise ratios from earthquakes with magnitudes larger than 5.7, depths less than 200 km, and distances between 60° and 80°. In total, 119 earthquakes were selected for analysis (Supplemental Table 1). The applied depth and distance criteria help to minimize any potentially interfering teleseismic phases (Wilson et al., 2006). Recorded waveforms are rotated from the north-east-vertical (N-E-Z) to the radial-transverse-vertical (R-T-Z) coordinate system using the event's back-azimuth and are visually inspected to pick the S-wave onset. Using Ligorria and Ammon's (1999) iterative time domain method, SRFs are generated by deconvolving the R component from the corresponding Z component, and both the time axes and the amplitudes of the SRFs are reversed to make the SRFs comparable to the more common PRFs (e.g. Kumar et al., 2005; Li et al., 2004). To improve the signal-to-noise ratio, individual SRFs were stacked at each station, and in general, each stack contains several tens of records (Supplemental Table 2).

Stacked SRFs for stations along several profiles through the GAMSEIS array (Fig. 1) are shown in Fig. 2. Some stations were temporarily offline, particularly in the coldest winter months, and did

Table 1
Summary of ice thickness estimates. Ice-penetrating radar measurements were only available for a few of the GAMSEIS stations (Blankenship et al., 2001; Kamiyama et al., 1994; D. Braaten and T. Jordan, personal communication). Ice thicknesses from BEDMAP (Lythe et al., 2001) are also shown for comparison.

Station name	Latitude (°)	Longitude (°)	Ice thickness from PRFs (km)	Ice thickness from radar (km)	Ice thickness from BEDMAP (km)
N124	−82.0745	107.6406	2.50	2.53	2.85
N132	−82.0751	101.9534	3.35	3.35	3.41
N140	−82.0086	96.7692	2.45	–	3.06
N148	−81.8625	91.5076	3.20	–	2.78
N156	−81.6726	86.5045	2.35	–	2.25
N165	−81.4084	81.7604	2.80	2.78	2.78
N173	−81.1122	77.4736	2.45	2.57	2.53
N182	−80.7363	73.1898	2.60	–	2.06
N190	−80.3275	69.431	3.25	–	3.18
N198	−79.8597	65.9607	2.85	–	3.09
N206	−79.3947	62.8556	2.40	–	3.06
N215	−78.9045	59.9943	2.75	–	3.30
P061	−84.4996	77.2238	2.90	2.82	2.97
P071	−83.6465	77.3347	2.10	1.97	2.84
P080	−82.8054	77.364	2.35	2.51	2.92
P090	−81.9361	77.3142	2.25	–	2.63
P116	−79.5669	77.0451	2.00	–	1.77
P124	−78.8718	77.657	1.30	1.55	1.41
GM01	−83.9858	104.7291	3.05	–	3.09
GM02	−79.4251	97.5815	2.90	–	2.80
GM03	−80.2169	85.9439	3.10	–	2.55
GM04	−82.9997	61.1124	2.95	–	3.06
GM05	−81.1841	51.1588	2.80	–	3.49
GM06	−79.3328	44.3148	3.15	–	3.66
GM07	−77.3136	39.6132	3.00	2.80	3.06
AGO1	−83.8596	129.6121	3.25	–	3.09

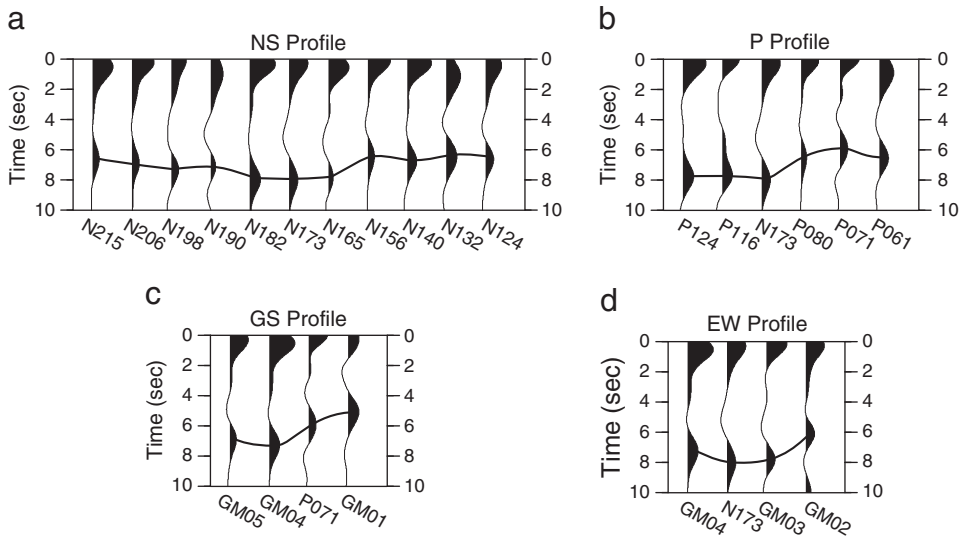

Fig. 2. Stacked SRFs along the (a) NS profile, the (b) P profile, the (c) GS profile, and the (d) EW profile. The black line denotes the Moho conversion beneath each station.

not record enough useable data to generate a stack with a high signal-to-noise ratio. Therefore, these stations are not shown. On each SRF stack, the initial arrival near 0 s is the direct S arrival combined with the Sp conversion from the base of the ice. The Gaussian width factor used in our analysis produces a fairly wide filter that causes the two signals to overlap (Hansen et al., 2009). The second arrival observed at each station is the Sp conversion from the Moho (Fig. 2). The timing of this conversion ranges between 5.1 s (station GM01) and 7.9 s (station N173), where the variability of the timing indicates variations in crustal thickness or velocity. For the two stations in common with the TAMSEIS deployment (stations N124 and N132), the SRF stacks shown in Fig. 2 are comparable to those from Hansen et al. (2009).

2.2. Estimating ice thickness

Ice thickness measurements are required to model our SRF data. However, unlike the Hansen et al. (2009) TAMSEIS study, ice thickness measurements from ice-penetrating radar were only available for a few of the GAMSEIS stations (Table 1; Blankenship et al., 2001; Kamiyama et al., 1994; D. Braaten and T. Jordan, personal communication). While ice thickness could be estimated from BEDMAP, the resolution of this model in East Antarctica is limited (Lythe et al., 2001). Therefore, estimates of the ice thickness had to be acquired with a more direct approach using the available seismic recordings.

For each GAMSEIS station, we also generated stacked PRFs using events with distances between 30° and 90° and with magnitudes ≥6.0 (Supplemental Table 3). The PRF stacks are dominated by multiples from the Ps conversion at the ice–rock interface (Fig. 3), which can be modeled to determine the ice thickness. Simple three-layer models, consisting of an ice layer, a 30-km thick crust, and an upper mantle half-space, were used to predict the timing of the first ice multiple at each station. The shear velocity (V_s) of the crust and upper mantle were set to 3.7 and 4.5 km/s, respectively. For stations where ice-penetrating radar data were available (Table 1; Blankenship et al., 2001; Kamiyama et al., 1994; D. Braaten and T. Jordan, personal communication), the V_s of the ice layer needed to be ~1.9 km/s in order to match the ice thickness measurements, which is reasonable given the general range of ice V_s determined by seismic experiments (1.5–2.0 km/s; Kim et al., 2007). Keeping the velocities fixed, the thickness of the ice at each remaining station was then determined by varying this parameter in the model until the predicted timing of the first ice multiple matched that observed on the corresponding PRF (Fig. 3). Ice thickness estimates are summarized in Table 1.

2.3. Estimating crustal thickness

To estimate the crustal thickness and mean crustal shear velocity, we model the Sp-S arrival times from the SRFs along with Rayleigh wave dispersion data. Phase velocities at periods between 18 and 30 s were obtained from the surface wave tomography model of Heeszel et al. (2010), who determined phase velocity maps at various frequencies using the two-plane wave method of Yang and Forsyth (2006). Similar to the Hansen et al. (2009) study, a grid search procedure was used to model both the SRFs and dispersion data. First, synthetic dispersion curves were generated for various velocity–depth models and were compared to the observed phase velocities. The velocity–depth models consisted of four layers: an ice layer, a two-layer crust, and an upper mantle half-space. For each station, the thickness of the ice layer was determined as outlined in the previous section and this thickness was fixed in the grid search (Table 1). The V_s of both the ice layer and the uppermost mantle were also fixed at 1.9 and 4.5 km/s, respectively. Moho depth was allowed to vary between 30 and 65 km in 1 km increments, and the crust was parameterized as two layers of equal thickness. The velocities in each crustal layer were averaged by slowness to equal a nominal mean crustal shear velocity ($\bar{V}_s$), which was varied

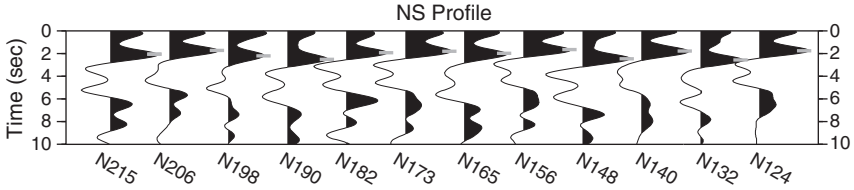

Fig. 3. Example PRF stacks from stations along the NS profile. The gray tick marks indicate the first Ps multiple from the ice–rock interface whose timing was used to determine the thickness of the ice layer at each station. Note the later arrival of this phase at stations such as N132 and N148, which have a thicker ice layer (Table 1).

between 3.4 and 3.9 km/s. In all models, the Poisson's ratio (σ) of the ice, crust, and upper mantle was set to 0.33, 0.25, and 0.28, respectively.

Given the uncertainty estimates provided by Heeszel et al. (2010), we conservatively examined the range of models whose predicted dispersion curves were within 0.08 km/s of the observed phase velocity data. For each station, the models that fit the associated dispersion data within error were examined further by comparing their predicted Moho Sp time to the observed Moho Sp time on the corresponding stacked SRF. The depth and distance of each event contributing to the stack at a given station were used to determine an average ray parameter (p). This p was then used to compute the vertical slowness for each layer in the model, which in turn was used to compute the predicted Sp-S time expected for the Moho conversion from that model. To account for variations in the ray parameter between different events contributing to the stack, an uncertainty of 0.3 s was assigned to the observed Moho Sp time. If the predicted Moho Sp time for a given model was within the uncertainty of the observed time, the model was accepted. An example of the data modeling is provided in Fig. 4.

2.4. Evaluating additional uncertainty

The range of models that fit both the observed dispersion data and the SRF Moho Sp time within the assigned error provide an estimate of the uncertainty associated with the crustal thickness and $\bar{V}_s$ results. An example of this is shown by the histograms in Fig. 4b and c. Across all examined stations, the standard deviations associated with the crustal thickness and $\bar{V}_s$ average 1.47 km and 0.04 km/s, respectively (Table 2).

However, additional uncertainties may also arise from the fixed parameters in the grid search. To assess how much the crustal thickness and $\bar{V}_s$ depend on the values chosen for these parameters, different ranges of ice thickness, ice V_s, and crustal σ were tested. While the ice thicknesses in our grid search were based on our PRF modeling (Section 2.2), the Sp conversion points at the base of the ice layer may not be located directly beneath the station. However, even for stations underlain by the thickest ice layer, such as station N132 where the ice is ~3.4 km thick, the Sp conversion points from the ice–rock interface are within 1.5 km of the station. Ice-penetrating radar measurements (Blankenship et al., 2001; D. Braaten and T. Jordan, personal communication) indicate that the ice thickness varies at most by ~0.2 km over this distance range. The ice V_s in our grid search was also based on our PRF modeling, but this velocity can vary over a wide range depending on the thickness of the firn layer. Seismic experiments indicate that the V_s of ice generally falls between about 1.5 and 2.0 km/s (Kim et al., 2007). Estimates of the σ for Antarctic crust were obtained from Finotello (2009), which fall between 0.24 and 0.27. On average, these ranges lead to a 2.5 km uncertainty in Moho depth and a 0.03 km/s uncertainty in $\bar{V}_s$. Combining these uncertainties with those associated with the dispersion data and the SRF Moho Sp times, we estimate that our $\bar{V}_s$ are resolved to within $\pm$0.07 km/s and our Moho depths are resolved to within $\pm$4 km.

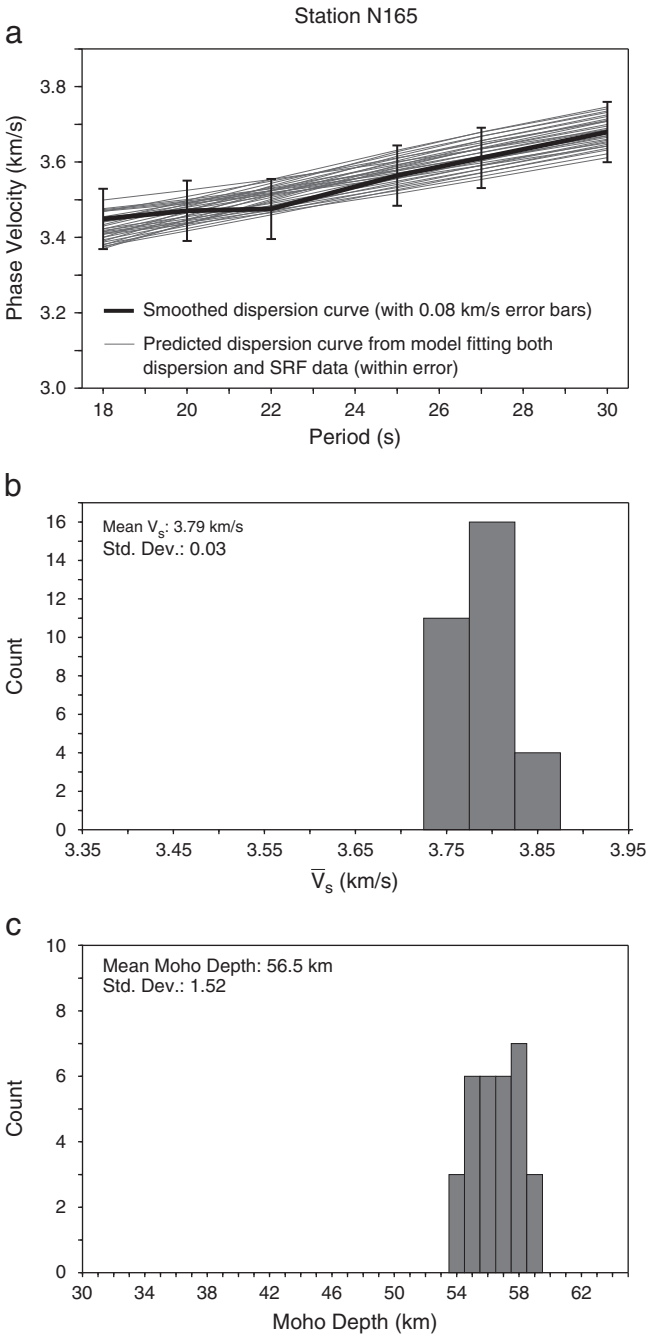

Fig. 4. Example of data modeling from station N165. (a) Gray lines show the predicted phase velocity dispersion curves for models that fit the dispersion data (Heeszel et al., 2010) within 0.08 km/s and that fit the SRF Moho Sp time within 0.3 s. (b) The range of mean crustal shear velocities ($\bar{V}_s$) encompassed by the "fit" models. (c) The range of Moho depths encompassed by the "fit" models. Note that these Moho depths include the thickness of the ice layer.

3. Results

Our crustal thickness estimates, in relation to bedrock and surface topography, are illustrated in Fig. 5 and summarized in Table 2. For the north–south (NS) profile, the plot has been extended further into the EA craton using the results of Hansen et al. (2009). For stations in common to both the GAMSEIS and TAMSEIS arrays, the crustal estimates from the current study match those found previously within the associated error bounds. As shown on the four different profiles (Fig. 5), crustal thickness beneath the EA craton surrounding the GSM averages ~40–45 km, agreeing well with many studies (e.g. Bentley, 1991; Hansen et al., 2009; Reading, 2006). However, beneath the GSM, the crust thickens to ~55–58 km. The $\bar{V}_s$ throughout the EA craton averages ~3.7 km/s, but a slightly faster $\bar{V}_s$ of ~3.8 km/s is observed within the GSM.

The $\bar{V}_s$ and crustal thickness estimates we obtain for the EA craton surrounding the GSM are comparable to those reported for other Precambrian terrains. For example, beneath the Archean Yilgarn craton in western Australia, crustal thickness varies from 36 to 46 km, with crustal V_s between 3.5 and 3.7 km/s (Goleby et al., 2004; Reading et al., 2003). In southern Africa, crustal V_s is fairly uniform, ranging from 3.5 to 3.75 km/s, but the crust is thinner (35–40 km) beneath some parts of the Archean Kaapvaal and Zimbabwe cratons and thicker (45–50 km) beneath Proterozoic mobile belts (e.g. Kgaswane

Table 2
Summary of mean crustal thickness and mean crustal shear velocity ($\bar{V}_s$) at each station, along with the associated standard deviations, determined using our grid search procedure.

Station name	Mean crustal thickness	Std. dev. of mean crustal thickness	$\bar{V}_s$	Std. dev. of $\bar{V}_s$
N124	45.0	1.48	3.70	0.04
N132	41.9	1.43	3.72	0.05
N140	46.2	1.42	3.76	0.04
N156	44.0	1.53	3.71	0.05
N165	53.7	1.52	3.79	0.03
N173	56.7	1.43	3.80	0.04
N182	55.7	1.54	3.80	0.04
N190	48.3	1.54	3.79	0.04
N198	50.3	1.53	3.81	0.04
N206	47.2	1.51	3.73	0.05
N215	44.6	1.51	3.71	0.05
P061	43.1	1.38	3.71	0.03
P071	40.2	1.49	3.64	0.05
P080	45.1	1.52	3.71	0.05
P116	54.9	1.37	3.80	0.04
P124	57.5	1.49	3.80	0.04
GM01	31.4	1.40	3.53	0.04
GM02	39.5	1.44	3.64	0.05
GM03	53.4	1.50	3.79	0.03
GM04	48.4	1.25	3.75	0.02
GM05	46.7	1.58	3.70	0.03

et al., 2009; Nair et al., 2006). These trends may also be observed on a global scale. Mooney et al. (1998) compiled 249 measurements of crustal thickness and velocity from Precambrian shields and showed there is little difference in crustal velocity between terrains of different age. They also argued that Archean terrains tend to have somewhat thinner crust (~40 km) compared to Proterozoic ones (~45–47 km). In contrast, Rudnick and Gao (2003), who also examined both Archean and Proterozoic terrains, found that crustal thickness ranges from 35 to 43 km regardless of age. The crustal thickness (~40–45 km) and $\bar{V}_s$ (~3.7 km/s) estimates we obtain for the EA craton are therefore consistent with those found globally for Precambrian terrains.

Our SRF results also provide the first well-constrained estimates of crustal thickness beneath the GSM. The ~55–58 km thick crust observed beneath the mountain range in the current study is in general agreement with several previous studies. For example, Groushinsky and Sazhina (1982a,b) compiled and modeled gravity data across Antarctica and also found indications of thick crust beneath the Gamburtsev massif, though their crustal estimates (~60–65 km) are thicker than those estimated here. von Frese et al. (1999) also estimated crustal thickness with gravity data and found a ~50 km thick crust beneath the GSM. Our results are also compatible with several ongoing seismic studies. Sun et al. (2009), who examined the 3D shear velocity structure of the crust and upper mantle across East Antarctica using the

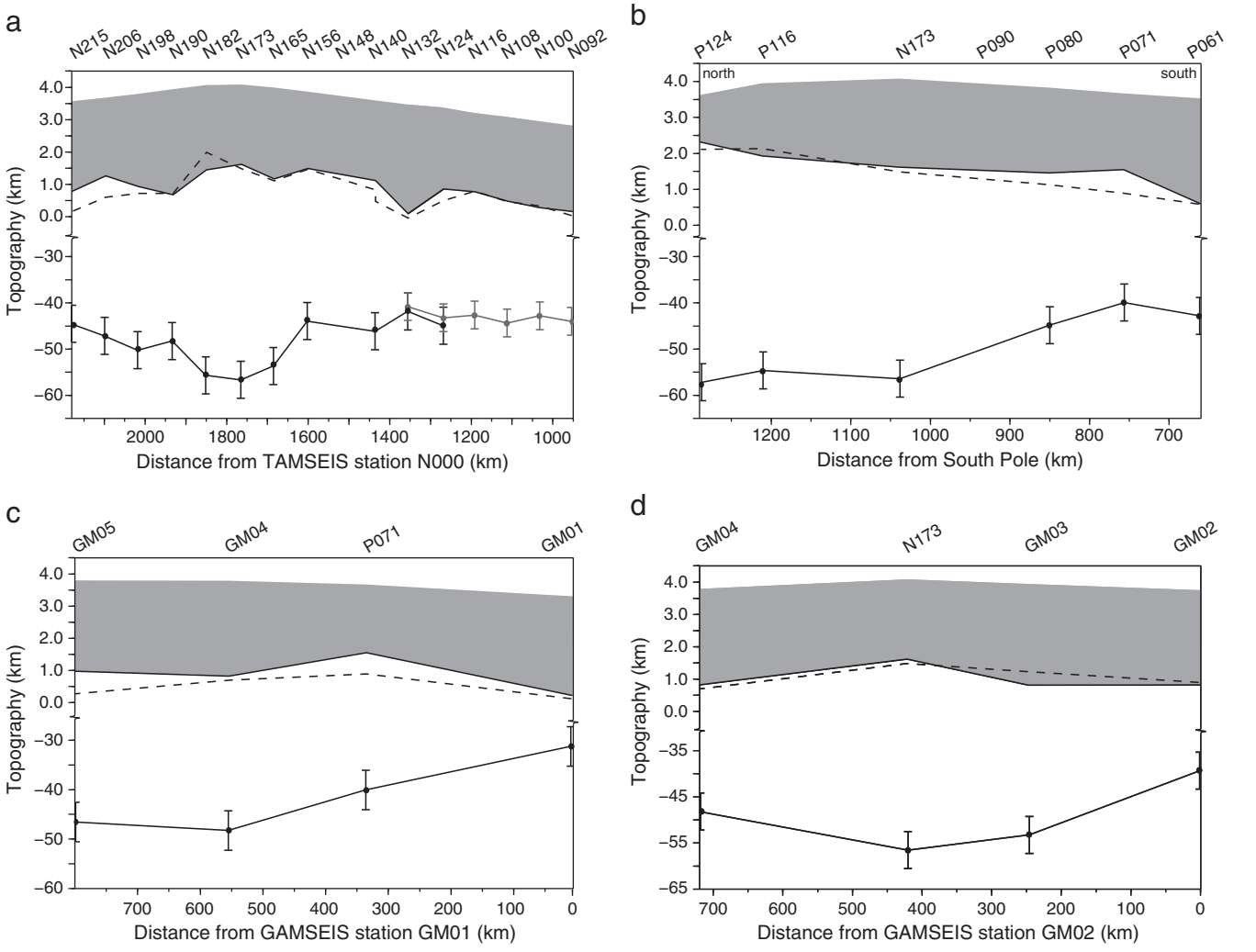

Fig. 5. Moho topography along the (a) NS, (b) P, (c) GS, and (d) EW GAMSEIS profiles. For all plots, the gray shaded area and solid black line indicate ice thickness and surface topography, respectively, determined using the PRF stacks. For comparison, the surface topography from BEDMAP (Lythe et al., 2001) is shown by the dashed black line. Our Moho depth estimates are shown by black dots with ±4 km error bars, as described in the text. Note the change of scale on the vertical axis. For the NS profile, the plot was extended further into the EA craton using the results of Hansen et al. (2009; gray dots with error bars).

cross-correlation of ambient seismic noise, found low crustal velocities extending to depths of ~60 km beneath the GSM, suggesting thickened crust. Heeszel et al. (2010) inverted Rayleigh wave phase velocities and found that crustal velocities extend to depths greater than 50 km beneath the central GSM, indicating a crustal root.

Several recent gravity studies, such as Block et al. (2009) and Llubes et al. (2003), indicate thinner crust beneath East Antarctica and the GSM, averaging ~37 km beneath the EA craton and ~43 km beneath the mountain range. The corresponding ~6 km of crustal thickening under the GSM is less than the ~13–18 km of crustal thickening indicated in our results. The cause of the discrepancy between the crustal thickness estimates determined with seismic versus gravimetric approaches is unclear; however, it may result from the starting crustal model used in the gravity analyses. The referenced gravity studies assumed a mean Moho depth of 35 km. If a deeper, starting Moho depth (~40–45 km; Bentley, 1991; Hansen et al., 2009; Reading, 2006) had been used, it is quite likely that the resulting crustal estimates would more closely match the seismic results. Additionally, Block et al. (2009) and Llubes et al. (2003) use topography and ice thickness measurements from the BEDMAP model, which has limited resolution in East Antarctica (Lythe et al., 2001).

4. Discussion

Our results indicate that the crust beneath the GSM is up to ~13–18 km thicker than the crust in the surrounding EA craton. Using the following relationship, we can estimate the expected topography resulting from isostatic compensation provided by the crustal root:

$$T = (\rho_c{}^{*}h) / (\rho_m - \rho_c).$$

In this equation, T is the thickness of the crustal root, ρ_c and ρ_m are the crustal and upper mantle densities, and h is the height of the isostatic topography (Turcotte and Schubert, 2002). Assuming ρ_c and ρ_m are 2.8 and 3.3 g/cm^3, respectively, a ~13–18 km thick crustal root leads to an additional 2–3 km of surface topography, matching that observed within the GSM well. Therefore, the thickened crust we observe appears to provide isostatic support for the high elevations in the GSM.

The origin of the crustal root beneath the GSM and therefore the origin of the mountains themselves still remain unresolved. Based on a study by Morelli and Danesi (2004), who estimated lithospheric thickness beneath Antarctica using surface wave tomography, Sleep (2006) pointed out that the GSM may coincide with an area of thin lithosphere within the EA craton. Sleep (2006) suggested that a mantle plume thinned the lithosphere beneath the GSM and uplifted the region. If this were the case, the thickened crust we observe could be explained by magmatic underplating associated with a mantle upwelling. However, more recent studies do not support the plume model. For example, Heeszel et al. (2010) found that upper mantle velocities beneath the GSM are faster than the global Preliminary Reference Earth Model (Dziewonski and Anderson, 1981) up to periods of 150 s, which would not be expected if the region had been thermally modified by a mantle upwelling. Instead, Heeszel et al. (2010) support the conclusion that the mountains are underlain by old, seismically fast cratonic lithosphere. This conclusion is also supported by other surface wave tomography studies (e.g. Ritzwoller et al., 2001; Shapiro and Ritzwoller, 2002). Ferraccioli et al. (2010) modeled aeromagnetic data across the GSM and found no evidence for magmatism in this region. van de Flierdt et al. (2008) dated detrital material deposited before the onset of glaciation in East Antarctica and thought to have originated from the GSM. They also find no evidence of young volcanic activity and suggest an old continental origin for the GSM.

If the GSM are a long-lived continental feature as the studies above suggest (Ferraccioli et al., 2010; Heeszel et al., 2010; van de Flierdt et al., 2008), the thickened crust we observe may date back to the late Proterozoic–early Paleozoic assembly of Gondwana. Liu et al. (2002, 2006) and Zhao et al. (1995) identified the Grove Mountains (72.8°S, 75.0°E) as a segment of the Pan-African age Prydz orogenic belt and suggested that the GSM were its inland continuation. Fitzsimons (2000, 2003) suggested that Cambrian outcrops near the Lambert Graben in the Southern Prince Charles Mountains are related to the 570–530 Ma Pinjarra Orogeny and may form a suture zone marked by thickened crust extending into the interior of East Antarctica beneath the GSM. Alternatively, the crustal structure of the GSM may have resulted from far-field collision and shortening associated with the assembly of Pangaea. Veevers (1994) suggested that stress from the Variscan orogeny acting on areas of weakened crust may have led to the uplift of the mountain range. In either case, it is difficult to reconcile the present elevation of the GSM with Proterozoic or Paleozoic tectonics because erosion should have long destroyed their relief. Therefore, the origin of the uplift and its history remain uncertain.

5. Conclusions

We have used SRFs and Rayleigh wave phase velocities to estimate the crustal structure beneath the EA craton and the GSM. The EA crust surrounding the GSM has an average thickness of ~40–45 km, consistent with estimates elsewhere for Precambrian crust. Beneath the GSM, the crust thickens to ~55–58 km and provides isostatic support for the mountain range. This thickened crust may reflect magmatic underplating associated with a mantle plume; however, given our results in conjunction with findings from other previous and ongoing studies, we favor models in which the GSM are an old continental feature associated with either Proterozoic or Paleozoic tectonic events.

Acknowledgements

We thank David Braaten from the Center for Remote Sensing of Ice Sheets (CReSIS) and Tom Jordan from the British Antarctic Survey for providing ice-penetrating radar measurements collected as part of the AGAP collaboration as well as Tim Parker, Guy Tytgat, Bruce Beaudoin, and the AGAP-GAMSEIS field crew for their efforts in collecting the data used in this study. We also thank Anya Reading and an anonymous reviewer for their thorough critiques of this manuscript. Portable seismic instrumentation for this project was obtained from the PASSCAL program of the Incorporated Research Institutions for Seismology (IRIS), and data handling assistance was provided by the IRIS Data Management System. Funding for this project was provided by the National Science Foundation grant numbers ANT-0537371, ANT-0537597, ANT-0838934, ANT-0838973, and ANT-0851560. Figures were prepared using GMT (Wessel and Smith, 1998).

Appendix A. Supplementary data

Supplementary data to this article can be found online at doi:10.1016/j.epsl.2010.10.022.

References

Bentley, C.R., 1991. Configuration and structure of the subglacial crust. In: Tingey, R.J. (Ed.), The Geology of Antarctica. Clarendon Press, Oxford, UK, pp. 335–364.

Blankenship, D.D., Morse, D.L., Finn, C.A., Bell, R.E., Peters, M.E., Kempf, S.D., Hodge, S.M., Studinger, M., Behrendt, J.C., Brozena, J.M., 2001. Geologic controls on the initiation of rapid basal motion for West Antarctic ice stream: a geophysical perspective including new airborne radar sounding and laser altimetry results. In: Bindschadler, R.A. (Ed.), The West Antarctic Ice Sheet: Behavior and Environment, Antarct. Res. Ser., 77. AGU, Washington DC, pp. 105–121.

Block, A.E., Bell, R.E., Studinger, M., 2009. Antarctic crustal thickness from satellite gravity: implications for the Transantarctic and Gamburtsev Subglacial Mountains. Earth Planet. Sci. Lett. 288, 194–203.
Bo, S., Siegert, M.J., Mudd, S.M., Sugden, D., Fujita, S., Xiang, C., Xueyuan, T., Yuansheng, L., 2009. The Gamburtsev mountains and the origin and early evolution of the Antarctic Ice Sheet. Nature 459. doi:10.1038/nature08024.
Cogley, J.G., 1984. Deglacial hypsometry of Antarctica. Earth Planet. Sci. Lett. 67, 151–177.
DeConto, R.M., Pollard, D., 2003. A coupled climate-ice sheet modeling approach to the early Cenozoic history of the Antarctic ice sheet. Palaeogeogr. Palaeoclimatol. Palaeoecol. 198, 39–52.
Dziewonski, A., Anderson, D., 1981. Preliminary reference earth model. Phys. Earth Planet. Int. 25, 297–356.
Ferraccioli, F., Bell, R., Damaske, D., Studinger, M., Braaten, D., Finn, C., 2010. Aerogeophysical exploration of the Gamburtsev Province during IPY. IPY Oslo Sci. Conf., Abstract LM8.5-3.
Finotello, M., 2009. Crustal structure along the Transantarctic Mountain Front using receiver functions. M.S. Thesis, The Pennsylvania State University.
Fitzsimons, I.C.W., 2000. Grenville-age basement provinces in East Antarctica: evidence for three separate collisional orogens. Geology 28, 879–882.
Fitzsimons, I.C.W., 2003. Proterozoic basement provinces of southern and south-western Australia, and their correlation with Antarctica. Geol. Soc. Spec. Pub. 206, 93–130.
Goleby, B., Blewett, R., Korsch, R., Champion, D., Cassidy, K., Jones, L., Groenewald, P., Henson, P., 2004. Deep seismic reflection profiling in the Archaean northeastern Yilgarn Craton, Western Australia: implications for crustal architecture and mineral potential. Tectonophysics 388, 119–133.
Groushinsky, N.P., Sazhina, N.B., 1982a. Some features of Antarctic crustal structure. Int. Union Geol. Sci. 4, 907–911.
Groushinsky, N.P., Sazhina, N.B., 1982b. Gravitational Field of Antarctica. Int. Union Geol. Sci. 4, 913–917.
Hansen, S.E., Julià, J., Nyblade, A.A., Pyle, M.L., Wiens, D.A., Anandakrishnan, S., 2009. Using S wave receiver functions to estimate crustal structure beneath ice sheets: an application to the Transantarctic Mountains and East Antarctic craton. Geochem. Geophys. Geosyst. 10. doi:10.1029/2009GC002576.
Heeszel, D.S., Sun, X., Wiens, D.A., Nyblade, A., Kanao, M., An, M., Zhao, Y., Anandakrishnan, S., Aster, R.C., 2010. Shear velocity structure of the Gamburtsev Mountains, Transantarctic Mountains, and East Antarctica from surface wave tomography. IPY Oslo Sci. Conf., Abstract PS1-D.91.
Kamiyama, K., Furukawa, T., Maeno, H., Kishi, T., Kanao, M., 1994. Glaciological data collected by the 33rd Japanese Antarctic Research Expedition in 1992. JARE DataRep., 194 (Glaciology 21), pp. 1–67.
Kgaswane, E., Nyblade, A., Julià, J., Dirks, P.H., Durrheim, R.J., Pasyanos, M.E., 2009. Shear wave velocity structure of the lower crust in southern Africa: evidence for compositional heterogeneity within Archaean and Proterozoic terrains. J. Geophys. Res. 114. doi:10.1029/2008JB006217.
Kim, K., Hong, M., Lee, J., Hong, J., Jin, Y., 2007. Seismic experiments on the Fourcade Glacier in the King George Island, Antarctica. Geophys. Res. Abs., EGU, 9, Abstract A-04755.
Kumar, P., Kind, R., Hanka, W., Wylegalla, K., Reigber, C., Yuan, X., Woelbern, I., Schwintzer, P., Fleming, K., Dahl-Jensen, T., Larsen, T.B., Schweitzer, J., Priestley, K., Gudmundsson, O., Wolf, D., 2005. The lithosphere–asthenosphere boundary in the North-west Atlantic region. Earth Planet. Sci. Lett. 236, 249–257.
Langston, C., 1979. Structure under Mount Rainier, Washington, inferred from teleseismic body waves. J. Geophys. Res. 83, 4749–4762.
Lawrence, J., Wiens, D., Nyblade, A., Anandakrishnan, S., Voigt, D., 2006. Crust and upper mantle structure of the Transantarctic Mountains and surrounding regions from receiver functions, surface waves, and gravity: implications for uplift models. Geochem. Geophys. Geosyst. 7. doi:10.1029/2006GC001282.
Li, X., Kind, R., Yuan, X., Wolbern, I., Hanka, W., 2004. Rejuvenation of the lithosphere by the Hawaiian plume. Nature 427, 827–829.
Ligorria, J., Ammon, C., 1999. Poisson's ratio variations of the crust beneath North America. Seismol. Res. Lett. 70, 274.
Liu, X., Zhao, Y., Liu, X., 2002. Geological aspects of the Grove Mountains, East Antarctica. Bull. R. Soc. NZ 35, 161–166.
Liu, X., Jahn, B., Zhao, Y., Li, M., Li, H., Liu, X., 2006. Late Pan-African granitoids from the Grove Mountains, East Antarctica: age, origin, and tectonic implications. Precambrian Res. 145, 131–154.
Llubes, M., Florsch, N., Legresy, B., Lemoine, J.-M., Loyer, S., Crossley, D., Rémy, F., 2003. Crustal thickness in Antarctica from CHAMP gravimetry. Earth Planet. Sci. Lett. 212, 103–117.
Lythe, M.B., Vaughan, D.G., Lambrecht, A., Miller, H., Nixdorf, U., et al., 2001. BEDMAP: a new ice thickness and subglacial topographic model of Antarctica. J. Geophys. Res. 106, 11335–11351.
Mooney, W., Laske, G., Masters, T., 1998. CRUST 5.1: A global crustal model at 5°×5°. J. Geophys. Res. 103, 727–747.
Morelli, A., Danesi, S., 2004. Seismological imaging of the Antarctic continental lithosphere: a review. Glob. Planet. Change 42, 155–165.
Nair, S., Gao, S., Liu, K., Silver, P., 2006. Southern African crustal evolution and composition: Constraints from receiver function studies. J. Geophys. Res. 111. doi:10.1029/2005JB003802.
Reading, A.M., 2006. The seismic structure of Precambrian and early Paleozoic terranes in the Lambert Glacier region, East Antarctica. Earth Planet. Sci. Lett. 244, 44–57.
Reading, A., Kennett, B., Dentith, M., 2003. Seismic structure of the Yilgarn Craton, West Australia. Aust. J. Earth Sci. 50, 427–438.
Ritzwoller, M.H., Shapiro, N.M., Levshin, A.L., Leahy, G.M., 2001. Crustal and upper mantle structure beneath Antarctica and surrounding oceans. J. Geophys. Res. 106, 30645–30670.
Roult, G., Rouland, D., 1992. Antarctica I: deep structure investigations inferred from seismology: a review. Phys. Earth Planet. Int. 84, 15–32.
Rudnick, R., Gao, S., 2003. Composition of the Continental Crust, in The Crust, Treatise on Geochemistry, edited by H.D. Holland and K.K. Turekian, Elsevier-Pergamon, Oxford, 3, 1–64.
Shapiro, N.M., Ritzwoller, M.H., 2002. Monte-Carlo inversion for a global shear velocity model of the crust and upper mantle. Geophys. J. Int. 151, 88–105.
Sleep, N.H., 2006. Mantle plumes from top to bottom. Earth Sci. Rev. 77, 231–271.
Sun, X., Wiens, D.A., Anandakrishnan, S., Aster, R.C., Huerta, A.D., Nyblade, A., Wilson, T.J., An, M., Kanao, M., 2009. Crust and upper mantle shear wave structure of Antarctica from seismic ambient noise. Eos Trans. AGU, 90(52), Fall Meet. Suppl., Abstract U51C-0046.
Turcotte, D.L., Schubert, G., 2002. Geodynamics, 2nd Ed. Cambridge University Press, New York, NY.
van de Flierdt, T., Hemming, S.R., Goldstein, S.L., Gehrels, G.E., Cox, S.E., 2008. Evidence against a young volcanic origin of the Gamburtsev Subglacial Mountains, Antarctica. Geophys. Res. Lett. 35. doi:10.1029/2008GL035564.
Veevers, J.J., 1994. Case for the Gamburtsev Subglacial Mountains of East Antarctica originating by mid-Carboniferous shortening of an intracratonic basin. Geology 22, 593–596.
Veevers, J.J., Saeed, A., Pearson, N., Belousova, E., Kinny, P.D., 2008. Zircons and clay from morainal Permian siltstone at Mt Rymill (73°S, 66°E), Prince Charles Mountains, Antarctica, reflect the ancestral Gamburtsev Subglacial Mountains–Vostok Subglacial Highlands complex. Gondwana Res. 14, 343–354.
von Frese, R.R.B., Tan, L., Kim, J.W., Bentley, C.R., 1999. Antarctic crustal modeling from the spectral correlation of free-air gravity anomalies with the terrain. J. Geophys. Res. 104, 25275–25296.
Watson, T., Nyblade, A., Wiens, D., Anandakrishnan, S., Benoit, M., Shore, P., Voigt, D., VanDecar, J., 2006. P and S velocity structure of the upper mantle beneath the Transantarctic Mountains, East Antarctic craton, and Ross Sea from travel time tomography. Geochem. Geophys. Geosyst. 7. doi:10.1029/2005GC001238.
Wessel, P., Smith, W., 1998. New, improved version of the generic mapping tools released. Eos Trans. AGU 79, 579.
Wilson, D., Angus, D., Ni, J., Grand, S., 2006. Constraints on the interpretation of S-to-P receiver functions. Geophys. J. Int. 165, 969–980.
Yang, Y., Forsyth, D.W., 2006. Regional tomographic inversion of amplitude and phase of Rayleigh waves with 2-D sensitivity kernels. Geophys. J. Int. 166, 1148–1160.
Zhao, Y., Song, B., Zhang, Z., Fu, Y., Chen, T., Wang, Y., Ren, L., Yao, Y., Li, J., Liu, X., 1995. Early Paleozoic (Pan African) thermal event of the Larsemann Hills and its neighbours, Prydz Bay, East Antarctica. Sci. Sin. 38, 74–84.
Zhu, L., Kanamori, H., 2000. Moho depth variation in Southern California from teleseismic receiver functions. J. Geophys. Res. 105, 2969–2980.